**Supplementary Table 1. Gene ontology Biofunctions pathways with the largest percentage of gene expression alterations in the basal ganglia of human HD individuals and PPARδ dominant-negative mice**

**Human HD caudate**

| | Biofunctions pathway | # of altered genes (% total) |
|---|---|---|
| | | |
| 1 | **CNS development and function** | 1170 (19.1) |
| 2 | **Molecular transport** | 970 (15.8) |
| 3 | **Lipid metabolism** | 524 (8.5) |
| 4 | **Huntington's Disease** | 421 (6.8) |
| 5 | **Neuritogenesis** | 329 (5.3) |
| 6 | **Neurotransmission** | 248 (4.0) |
| 7 | **neuronal differentiation** | 191 (3.1) |
| 8 | **cAMP-Protein Kinase (PKA) signaling** | 177 (2.8) |
| 9 | **axonal guidance** | 122 (2.0) |
| 10 | **G-protein coupled receptors** | 120 (1.9) |

**Mouse PPARδ$^{E411P}$ striatum**

| | Biofunctions pathway | # of altered genes (% total) |
|---|---|---|
| | | |
| 1 | **CNS development and function** | 142 (24.4) |
| 2 | **Molecular transport** | 142 (24.4) |
| 3 | **Lipid metabolism** | 80 (13.7) |
| 4 | **Huntington's Disease** | 44 (7.5) |
| 5 | **Neuritogenesis** | 41 (7.0) |
| 6 | **Ca2+ related** | 34 (5.8) |
| 7 | **Neurotransmission** | 29 (4.9) |
| 8 | **neuronal differentiation** | 23 (3.9) |
| 9 | **cAMP-Protein Kinase (PKA) signaling** | 17 (2.9) |
| 10 | **axonal guidance** | 16 (2.7) |

## Supplementary Table 2. Brain penetration of KD3010 after systemic delivery

| Plasma Concentration of KD3010 after IP Administration (ng/mL) | | | |
|---|---|---|---|
| **IP Time (hrs)** | **Mean IP** | **SD** | **CV (%)** |
| 2.00 | **7263** | **1341** | **18.5** |
| 8.00 | **961** | **359** | **37.3** |
| 24.0 | **46.6** | **41.4** | **88.8** |
| **Brain Concentration of KD3010 after IP Administration (ng/g)^** | | | |
| **IP Time (hrs)** | **Mean IP** | **SD** | **CV (%)** |
| 2.00 | **912** | **211** | **23.1** |
| 8.00 | **88.3** | **25.9** | **29.3** |
| 24.0 | **4.87** | **ND** | **ND** |

**ND** = not determined

**^Brain Concentration (ng/g)** = Brain Homogenate Concentration (ng/mL) × 5 (dilution factor)

| Brain/Plasma Ratio[#] of KD3010 | | | |
|---|---|---|---|
| **IP Time (hrs)** | **Mean IP** | **SD** | **CV (%)** |
| 2.00 | **0.126** | **0.0255** | **20.2** |
| 8.00 | **0.0942** | **0.00919** | **9.75** |
| 24.0 | **0.105** | **ND** | **ND** |

[#]**Brain/Plasma Ratio** = Brain Concentration (ng/g) / Plasma Concentration (ng/mL)

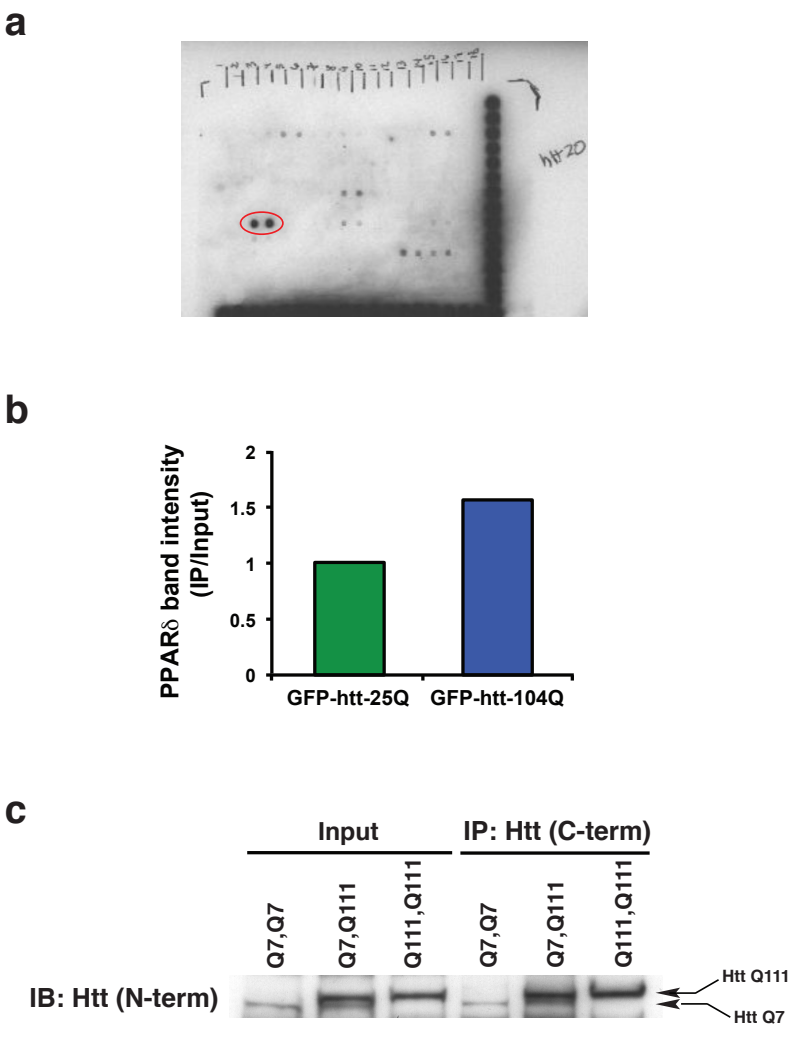


**Supplementary Figure 1**

**Identification and validation of a physical interaction between huntingtin and PPARδ.**
(a) Here we see the results of an unbiased screen for huntingtin (htt) protein interactors using the Panomics transcription factor (TF) immunoprecipitation (IP) array. We prepared nuclear extract from HEK293 cells expressing htt-Q25, and after incubating the nuclear extract with biotin-labeled probes corresponding to a library of transcription factor binding sites, we performed an immunoprecipitation with a htt-specific antibody, and then applied the immunoprecipitated material to the TF IP array. The most intense hybridization signal was obtained for the PPRE sequence (circled in red).
(b) Quantification of signal intensity for PPARδ in HEK293 cell co-transfection experiments comparing immunoprecipitation of PPARδ with a GFP-specific antibody from GFP-htt-25Q-expressing cells and from GFP-htt-104Q-expressing cells. The polyQ expansion tract favors a more pronounced interaction.
(c) Immunoprecipitation of ST-*Hdh* striatal-like neurons of the indicated genotypes was performed with a htt-specific antibody directed against a C-terminal epitope of the htt protein, followed by immunoblotting for htt protein with a htt-specific antibody directed against a N-terminal epitope. Note detection of both normal full-length htt-Q7 and polyglutamine-expanded full-length htt-Q111 proteins, thereby validating the C-terminal antibody for htt immunoprecipitation.

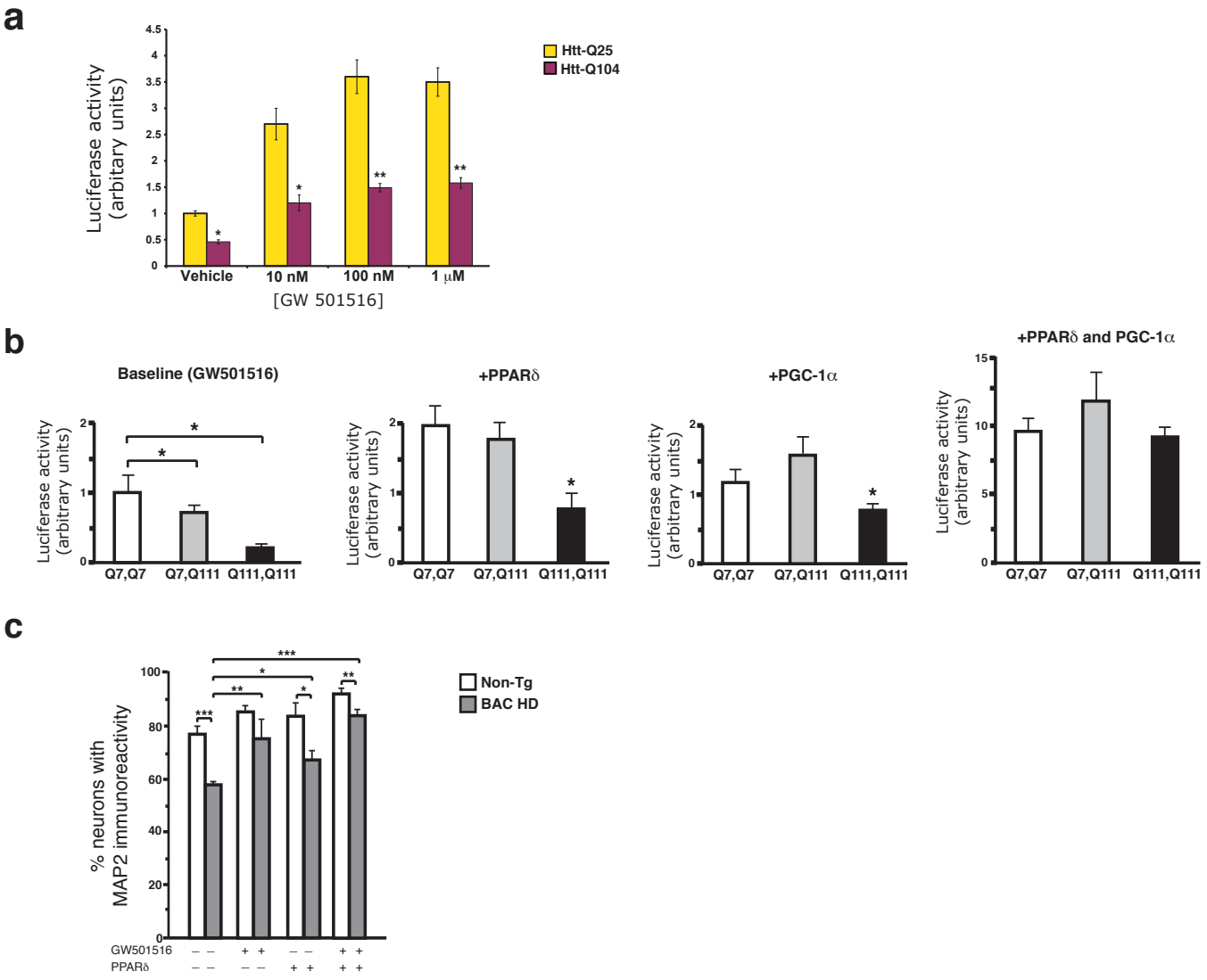


**Supplementary Figure 2**

**PolyQ-htt repression of PPARδ transactivation, and rescue of polyQ-htt neurotoxicity by PPARδ.** (a) HEK293 cells were co-transfected with a 3X-PPRE luciferase reporter construct, Renilla luciferase vector, and the htt-Q25 or htt-Q104 expression construct, as indicated, and treated with increasing concentrations of GW501516 agonist. Expression of polyQ-htt protein significantly repressed PPARδ-transactivation at baseline and at all tested GW501516 concentrations. $^{**}P < .01$, $^{*}P < .05$; t-test. (b) ST-*Hdh* striatal-like neurons were co-transfected with a 3X-PPRE luciferase reporter construct, Renilla luciferase vector, and PPARδ and/or PGC-1α expression constructs, as indicated, and treated with GW501516 (100 nM) as agonist. Co-transfection of PPARδ or PGC-1α alone rescues PPARδ transactivation in Q7/Q111 striatal-like neurons, but not in Q111/Q111 cells, while co-transfection of PPARδ and PGC-1α together yields complete rescue, and drives super-induction of PPRE activity. All results were normalized to Q7/Q7 cells at baseline. $^{*}P < .05$; ANOVA with post-hoc Tukey test. (c) Primary cortical neurons from BAC-HD and Non-Tg mice were vehicle-treated or co-transfected with PPARδ in the presence of GW501516 agonist, as indicated. We immunostained for microtubule-associated protein 2 (MAP2). At baseline, BAC-HD neurons display decreased MAP2 staining, which is rescued by GW501516 agonist treatment or co-transfection of PPARδ, and most improved by combined GW501516 agonist treatment and PPARδ co-transfection. Non-Tg neurons exhibit significantly greater MAP2 immunoreactivity than BAC-HD neurons, except with GW501516 treatment. All results were normalized to Non-Tg neurons at baseline. $^{***}P < .001$, $^{**}P < .01$, $^{*}P < .05$; t-test. Error bars = s.e.m.

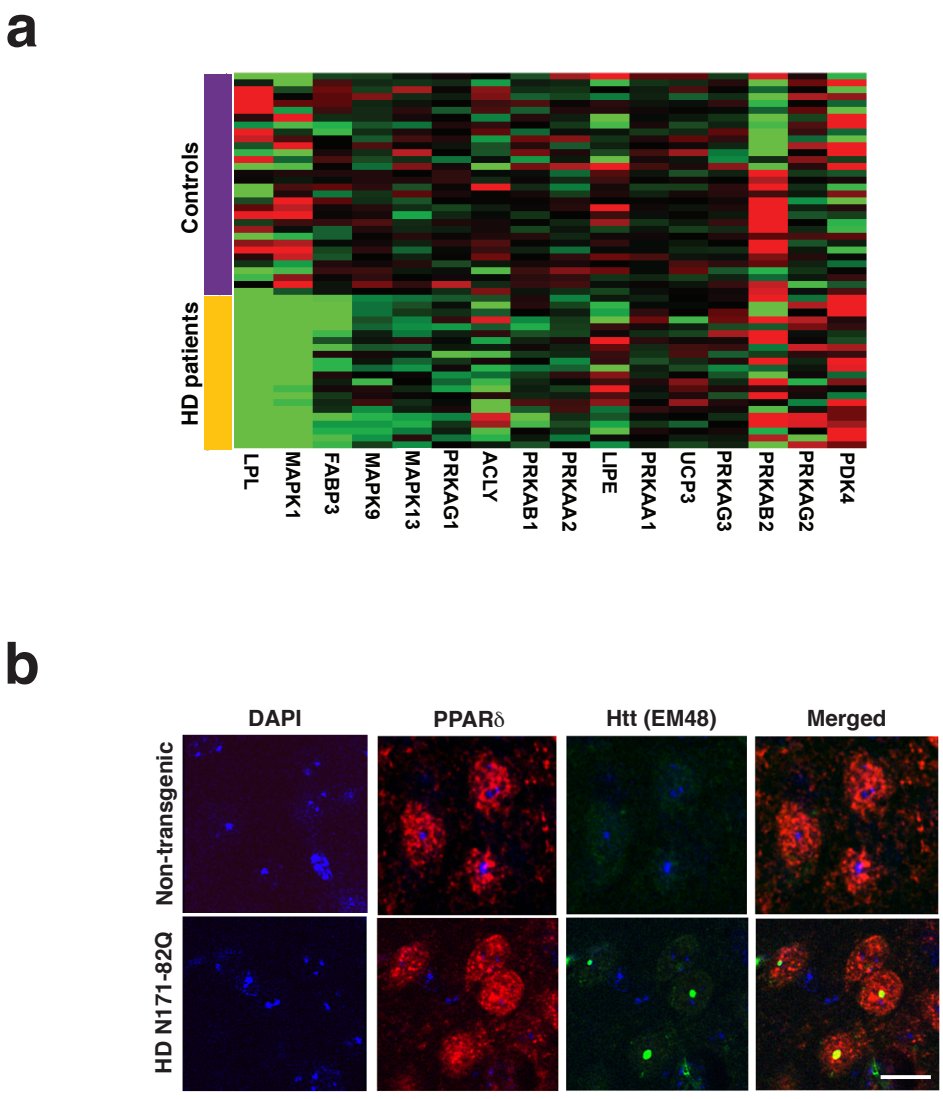


**Supplementary Figure 3**

**Altered expression of PPARδ-regulated genes in human HD caudate, and co-localization of PPARδ and polyQ-huntingtin in neuronal nuclei.**
(a) Here we see a heat map comparing the caudate nucleus expression of 16 PPARδ target genes for 22 Grade 0 – 2 HD patients (adjacent to gold bar) and 32 matched controls (adjacent to purple bar). Note that intensity of red signal corresponds to degree of relative up-regulation, while intensity of green signal corresponds to degree of relative down-regulation. The expression levels of 12 out of 16 PPARδ target genes are significantly altered in HD patients ($P < 10^{-4}$; $\chi 2$). The fact that 4 of the 16 are not significantly altered likely reflects the fact that this list of PPARδ target genes is derived from expression studies performed in skeletal muscle, since the regulome of PPARδ in the CNS is yet to be defined.
(b) Sections of striatum from 18 week-old HD N171-82Q transgenic mice and non-transgenic controls were immunostained with a PPARδ-specific antibody (red) and the htt-specific antibody EM48 (green), and counterstained with DAPI (blue). Merged images reveal co-localization of htt and PPARδ in HD transgenic striatum. Scale bar = 10 μM.

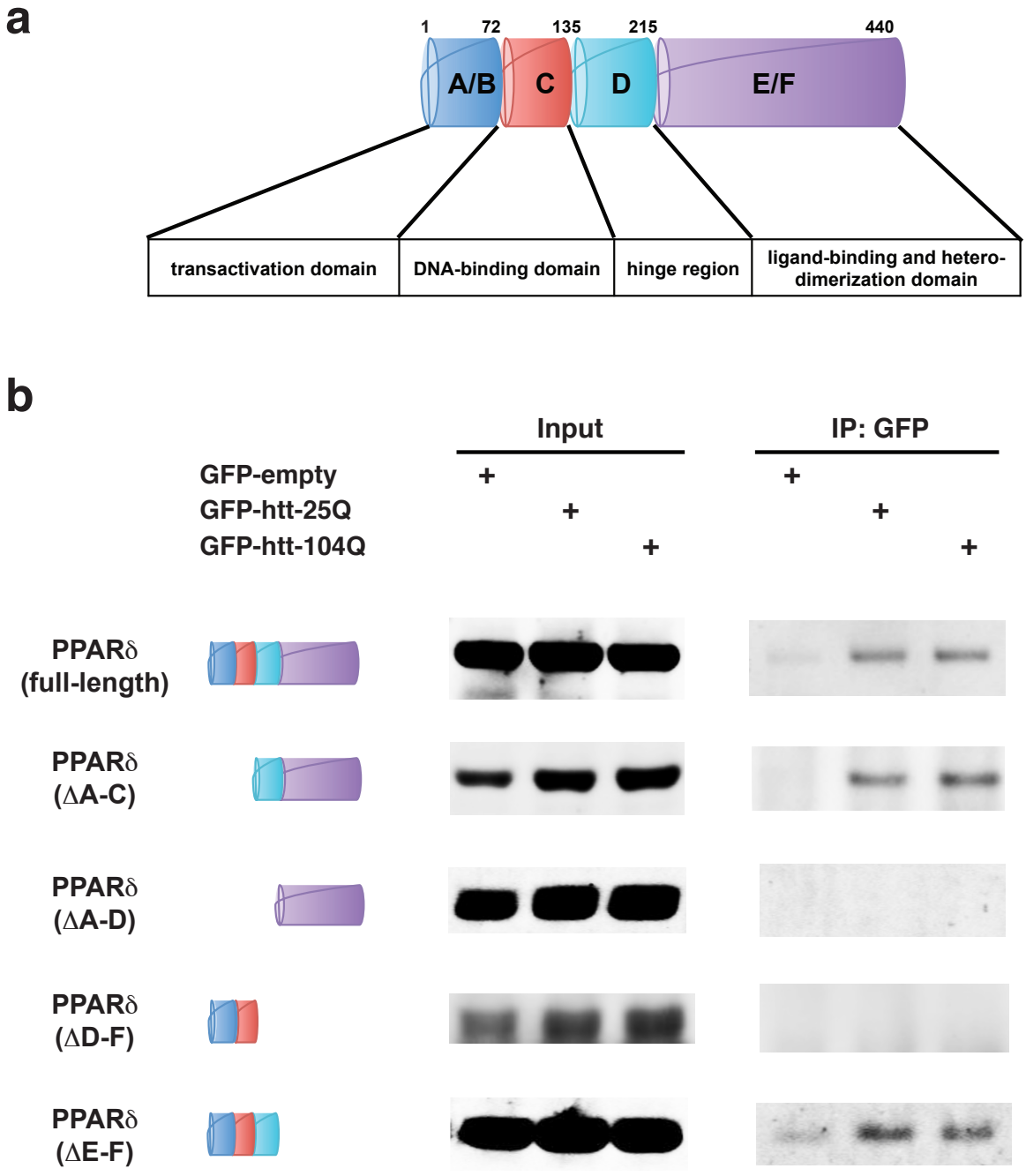


**Supplementary Figure 4**

**Mapping of the huntingtin interaction site on PPARδ.**

(a) Diagram of PPARδ highlighting its functional domains.
(b) HEK293 cells were co-transfected with GFP-empty vector, GFP-htt-25Q or GFP-htt-104Q and PPARδ-Flag or a PPARδ-Flag deletion construct, as indicated. Immunoprecipitation was performed with a GFP-specific antibody, followed by immunoblotting for Flag. GFP-empty served as a negative control, and full-length PPARδ served as a positive control.

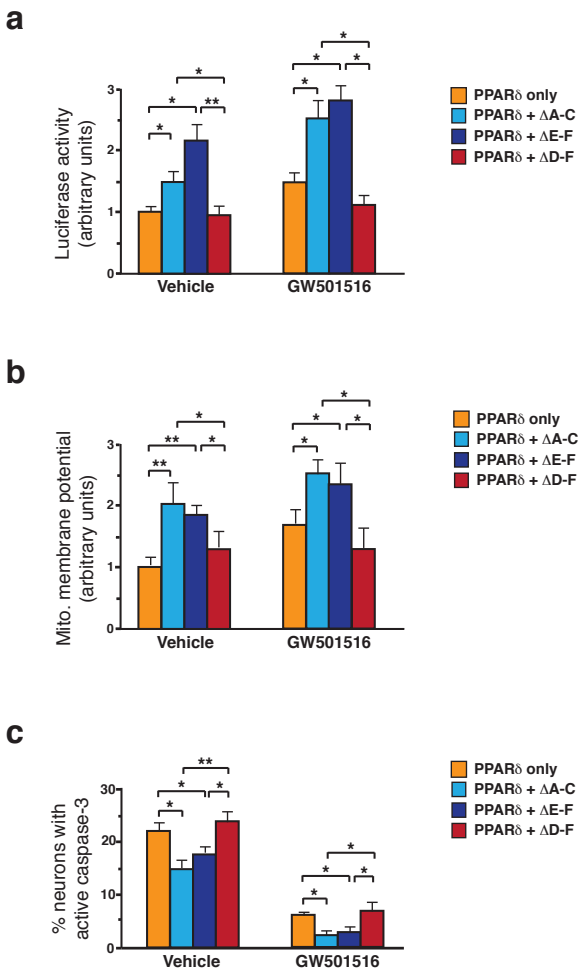


**Supplementary Figure 5**
**Physical interaction of polyQ-htt with PPARδ underlies HD neurotoxicity.**

(a) ST-*Hdh* Q111/Q111 striatal-like neurons were co-transfected with a 3X-PPRE luciferase reporter construct, Renilla luciferase vector, and PPARδ in combination with a PPARδ deletion construct, as indicated, and treated with GW501516 as agonist. At baseline, 3x-PPRE luciferase reporter activity is repressed as a function of htt Q length. Co-transfection of PPARδ lacking either the A – C domain or the E – F domain rescues PPARδ transcription repression, but co-transfection of PPARδ lacking the D – F domain does not rescue PPARδ transcription repression. All results were normalized to Q111/Q111 cells transfected with only PPARδ and treated with vehicle. $*P < .05$, $**P < .01$; ANOVA with post-hoc Tukey test. (b) ST-*Hdh* Q111/Q111 striatal-like neurons were co-transfected with PPARδ in combination with a PPARδ deletion construct, as indicated, treated with GW501516 as agonist, and exposed to JC-1 dye to measure mitochondrial membrane potential. Co-transfection of PPARδ lacking either the A – C domain or the E – F domain rescues mitochondrial membrane potential, but co-transfection of PPARδ lacking the D – F domain does not. All results were normalized to Q111/Q111 cells transfected with only PPARδ and treated with vehicle. $*P < .05$, $**P < .01$; ANOVA with post-hoc Tukey test. (c) ST-*Hdh* Q111/Q111 striatal-like neurons were co-transfected with PPARδ in combination with a PPARδ deletion construct, as indicated, treated with GW501516 as agonist, and immunostained for active caspase-3. Co-transfection of PPARδ lacking either the A – C domain or the E – F domain prevents cell death, but co-transfection of PPARδ lacking the D – F domain does not. All results were normalized to Q111/Q111 cells transfected with only PPARδ and treated with vehicle. $*P < .05$, $**P < .01$; ANOVA with post-hoc Tukey test. Error bars = s.e.m.

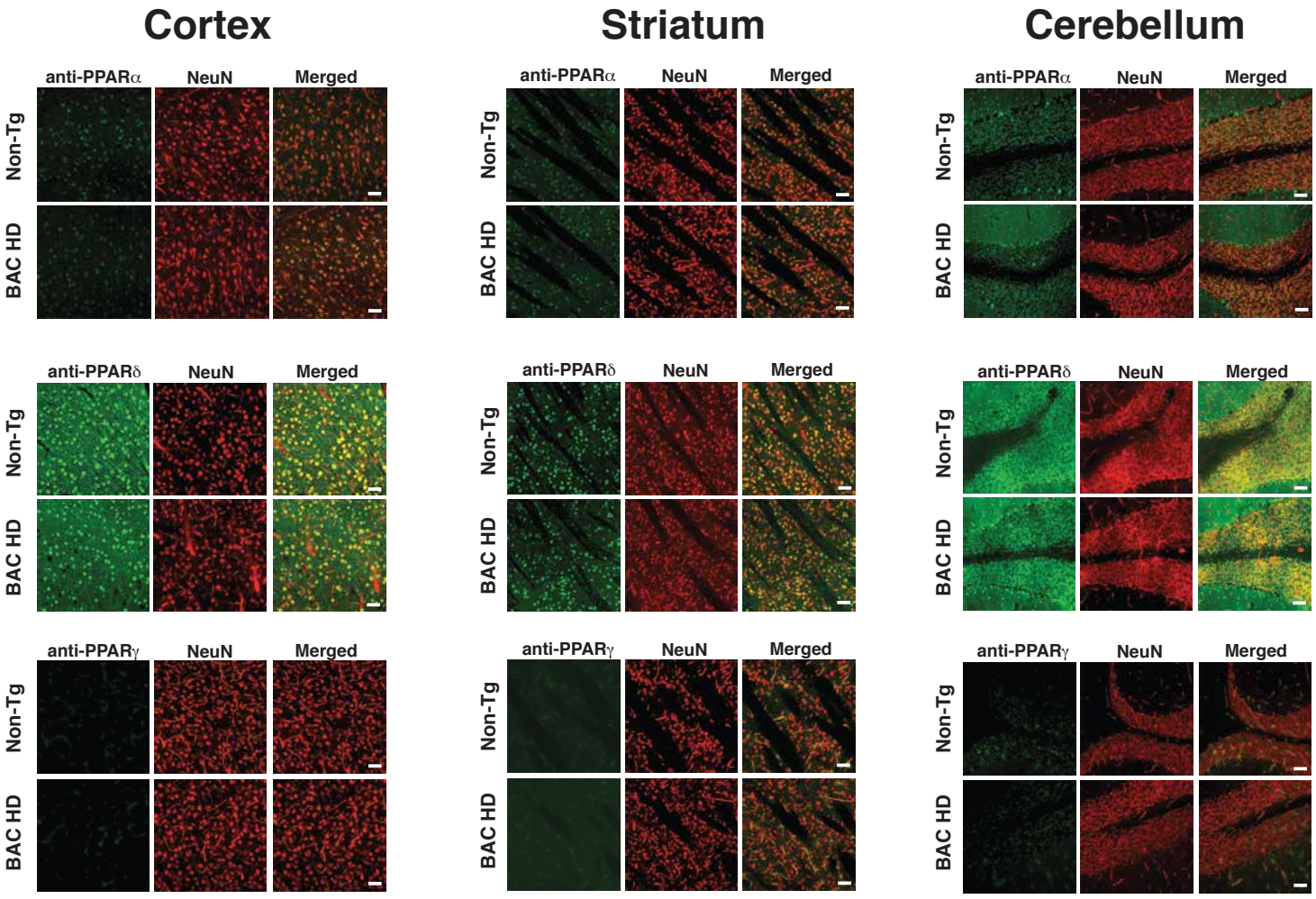


**Supplementary Figure 6**

**Expression of the different PPARs in neurons of the cortex, striatum, and cerebellum.**

Sections of cortex (left), striatum (center), and cerebellum (right) from one year-old non-transgenic (Non-Tg) control mice and from BAC-HD mice were immunostained with the indicated the PPAR-specific antibody (green) and a NeuN-specific antibody (red). Merged images reveal expression of indicated PPAR in neurons of the indicated brain region. Scale bars = 10 μM.

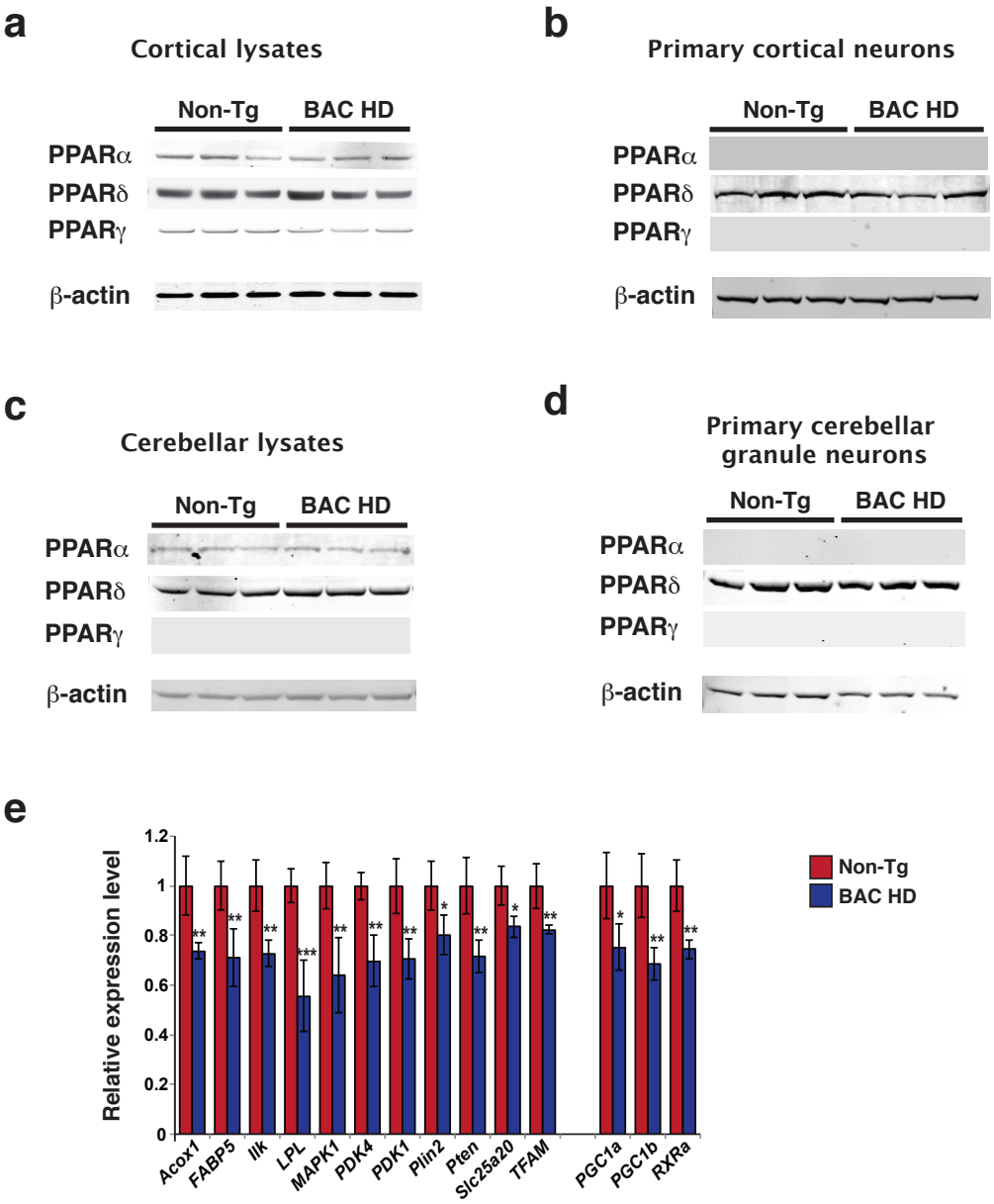


**Supplementary Figure 7**

**Survey of PPAR protein expression in CNS, and of PPARδ target gene RNAs in BAC-HD mice.** (a) Immunoblotting of cortical lysates from one year-old BAC-HD mice and non-transgenic (Non-Tg) littermate controls. (b) Immunoblotting of primary cortical neurons obtained from BAC-HD mice and Non-Tg littermates. (c) Immunoblotting of cerebellar lysates from one year-old BAC-HD mice and Non-Tg littermates. (d) Immunoblotting of primary cerebellar granule neurons obtained from BAC-HD mice and Non-Tg littermate controls. β-actin served as the loading control for all immunoblot experiments. (e) RT-PCR analysis of PPARδ target gene expression and co-activator expression in the striatum of 8 month-old BAC HD and Non-Tg (n = 4 mice / genotype; 6 technical replicates). $^{**}P < .01$, $^{*}P < .05$; t-test. Error bars = s.e.m.

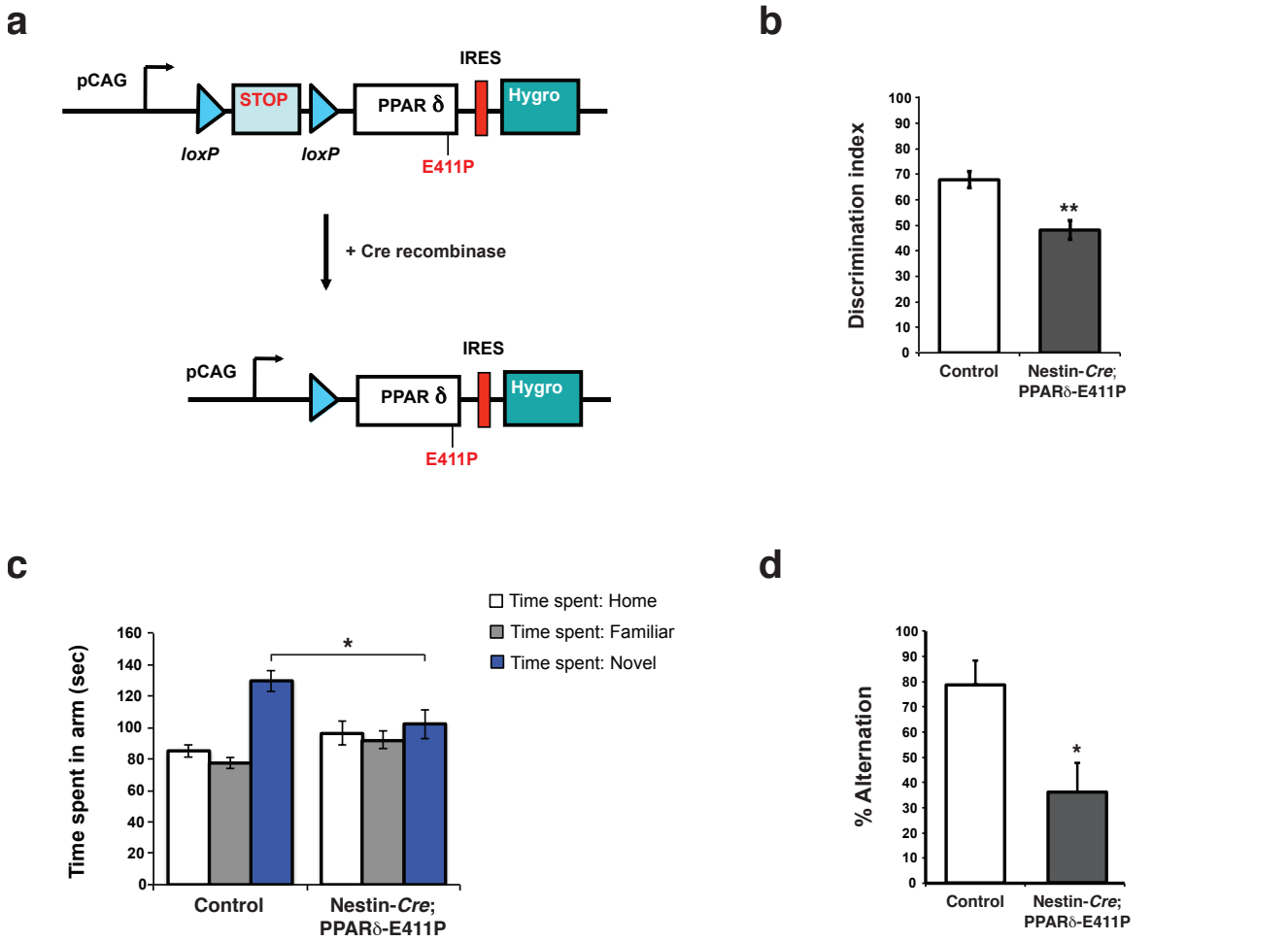


**Supplementary Figure 8**

**Nestin-Cre;PPARδ-E411P mice exhibit deficits of learning and memory.**

(a) Diagram of the conditional PPARδ transgenic expression construct. We inserted a PPARδ cDNA containing a single nucleotide mutation, resulting in substitution of proline for glutamate at amino acid position 411, in the CAGGS transgenic expression system (pCAG), which consists of a β-actin promoter and CMV enhancer. To restrict expression of dominant-negative PPARδ E411P to specific cell types, we placed a transcriptional STOP cassette 5' to the PPARδ cDNA and flanked the STOP cassette with loxP sites. In the presence of Cre recombinase, the STOP cassette is excised, permitting high-level expression of the PPARδ E411P gene product.

(b) 10 month-old Nestin-Cre;PPARδ-E411P mice and littermate control mice were habituated to an open field apparatus and then exposed to two identical objects. The next day the mice were exposed to two objects, one identical to the prior object and one novel. The time spent exploring the novel object divided by total exploration time was calculated as the discrimination index. $^{**}P < .01$, t-test.

(c) 10 month-old Nestin-Cre;PPARδ-E411P mice and non-transgenic littermate control mice were placed in a three-armed Y maze, and time spent exploring different arms of the maze was measured. Control mice demonstrated a preference for exploring the novel arm compared to the Nestin-Cre;PPARδ-E411P mice. $^{*}P < .05$, t-test.

(d) 10 month-old Nestin-Cre;PPARδ-E411P mice and non-transgenic littermate control mice were placed in a three-armed Y maze, and the number of successive entries into a different arm out of the total number of arm entries (in triads) was calculated as the % alternation. $^{*}P < .05$, t-test.

Group sizes were: 14 control mice and 8 Nestin-Cre;PPARδ-E411P mice. Error bars = s.e.m.

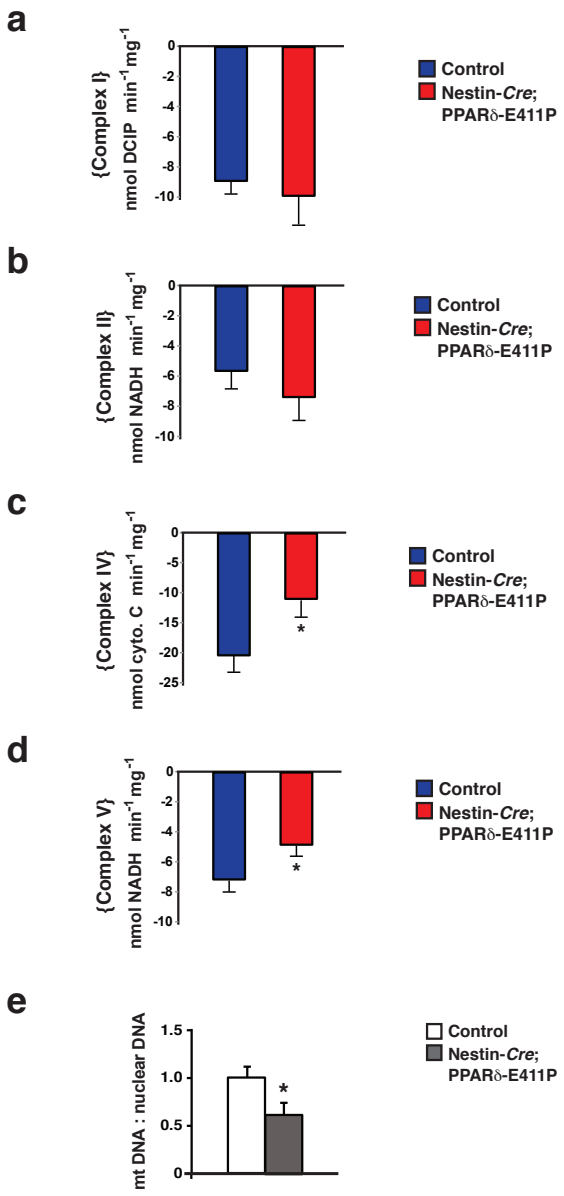


**Supplementary Figure 9**
**Analysis of mitochondrial function and bioenergetics in Nestin-Cre;PPARδ-E411P mice.**

(**a**) We measured mitochondrial complex I activity in the striatum of 8 month-old Nestin-Cre;PPARδ-E411P mice and littermate controls (n = 3 mice / group) by assaying the reduction of DCIP. Complex I activities are similar. (**b**) We measured mitochondrial complex II activity in the striatum of 8 month-old Nestin-Cre;PPARδ-E411P mice and littermate controls (n = 3 mice / group) by assaying the reduction of NADH. Complex II activities are similar. **(c)** We measured mitochondrial complex IV activity in the striatum of 8 month-old Nestin-Cre;PPARδ-E411P mice by assaying the reduction of cytochrome C, and observed reduced complex IV activity in Nestin-Cre;PPARδ-E411P mice in comparison to littermate controls (n = 3 mice / group). *$P < .05$; t-test. **(d)** We measured mitochondrial complex V activity in the striatum of 8 month-old Nestin-Cre;PPARd-E411P mice by assaying the reduction of NADH, and observed reduced complex V activity in Nestin-Cre;PPARδ-E411P mice in comparison to littermate controls (n = 3 mice / group). *$P < .05$; t-test. (**e**) We measured mitochondrial DNA copy number in the striatum of 8 month-old Nestin-Cre;PPARδ-E411P mice by performing real-time DNA PCR on a mitochondrial genome amplicon and nuclear genome amplicon. We detected significantly decreased mitochondrial DNA copy number in Nestin-Cre;PPARδ-E411P mice (n = 3 mice / group). *$P < .05$; t-test. Error bars = s.e.m.

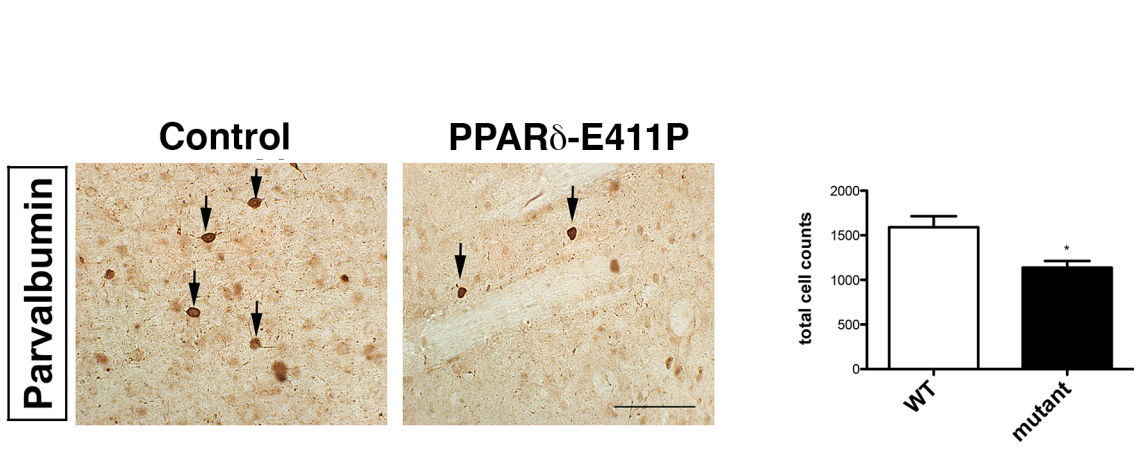


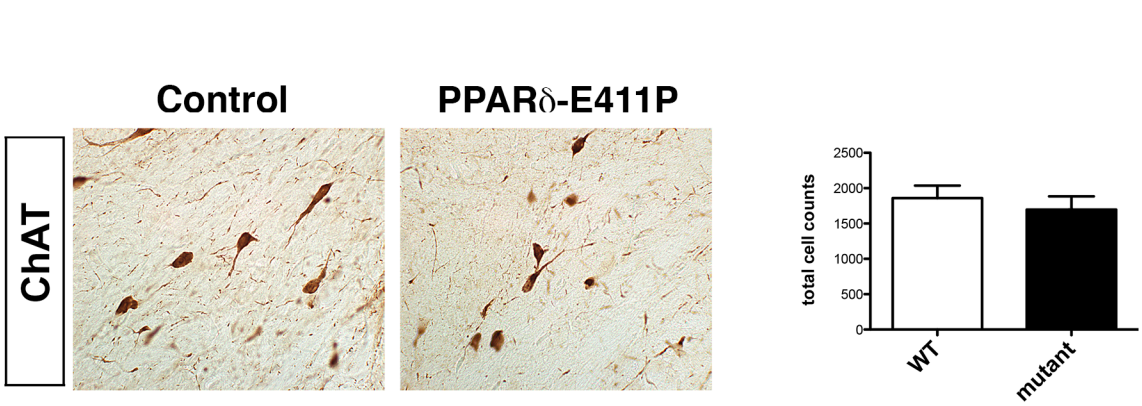


**Supplementary Figure 10**

**Rgs9-Cre;PPARδ-E411P mice exhibit loss of parvalbumin positive neurons in the striatum.**

(a) Sections of striatum from 10 month-old Rgs9-Cre;PPARδ-E411P mice and littermate controls were immunostained for parvalbumin to visualize neurons. Quantification of parvalbumin-positive neurons is shown on the right $^{*}P < .05$; t-test.
(b) Sections of striatum from 10 month-old Rgs9-Cre;PPARδ-E411P mice and non-transgenic littermate controls were immunostained for choline acetyltransferase to visualize neurons. Quantification of acetylcholinesterase-positive neurons is shown on the right.
n = 4 mice / group. Error bars = s.e.m. Scale bar = 40 μM.

**a**

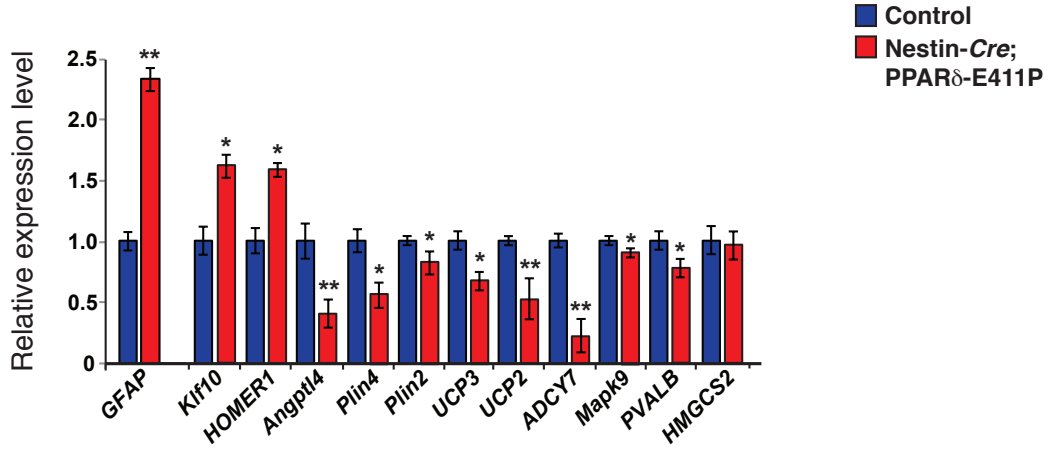


**b**

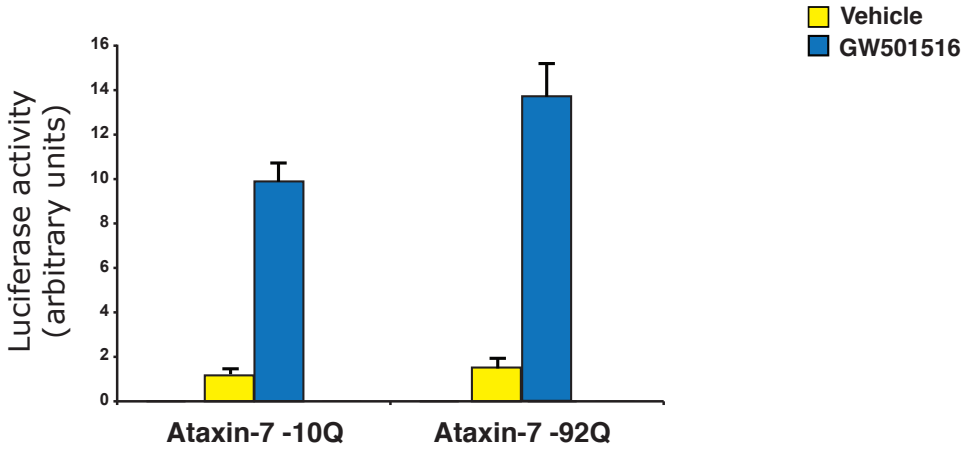


**Supplementary Figure 11**

**RNA-Seq transcriptome validation and specificity of PPARδ repression.**

(a) RT-PCR analysis of striatal RNAs (n = 3 mice / genotype; 9 technical replicates) for a subset of 11 significantly altered genes identified from RNA-Seq analysis of Nestin-Cre;PPARδ-E411P mouse striatum. RT-PCR analysis of GFAP expression serves as a positive control.
$^{**}P < .01$, $^{*}P < .05$; t-test. Error bars = s.e.m.
(b) HEK293 cells were co-transfected with a 3X-PPRE luciferase reporter construct, Renilla luciferase vector, and the ataxin-7-10Q or ataxin-7-92Q expression construct, as indicated, and treated with GW501516 agonist. Expression of polyQ-expanded ataxin-7 protein did not repress PPARδ-dependent transactivation, but actually showed a trend toward increased transactivation. Error bars = s.e.m.

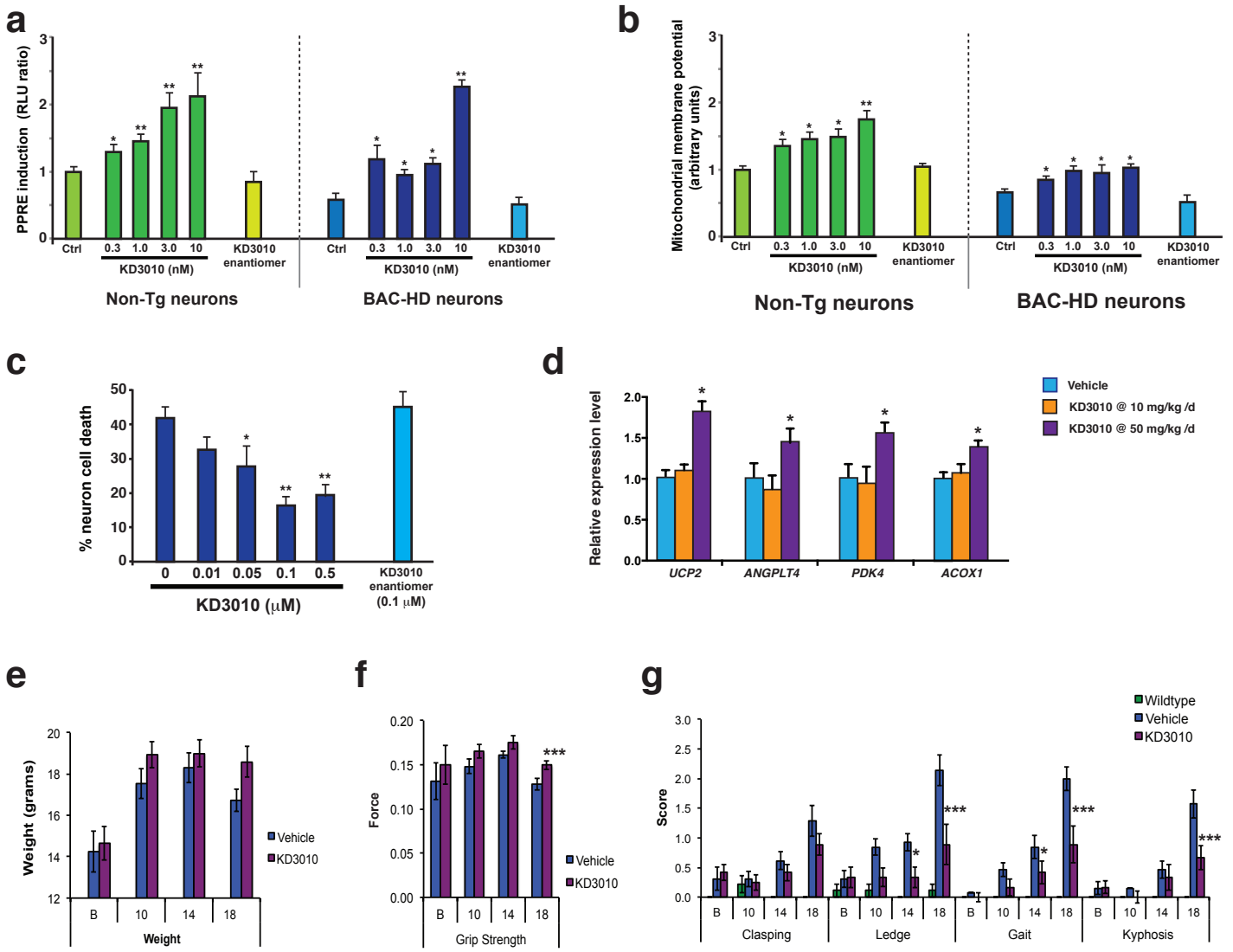


**Supplementary Figure 12**

**KD3010 rescues mutant htt toxicity *in vitro* and *in vivo*.**

(a) Wild-type or BAC-HD cortical neurons were co-transfected with PPARδ, 3xPPRE-luciferase, and Renilla-luciferase, and treated with KD3010, or inactive enantiomer. (b) Wild-type or BAC-HD cortical neurons were treated with KD3010, or inactive enantiomer, and cultured with JC-1 dye. For (a) and (b), control (Ctrl) runs indicate neurons not treated with KD3010, and results are normalized to wild-type neurons at baseline, which was set to 1. $*P < 0.05$, $**P < 0.01$; ANOVA with post-hoc Tukey test. (c) Wild-type cortical neurons were transfected with a 586 amino acid N-terminal htt fragment containing 82 glutamines, and treated with KD3010 or inactive enantiomer. $*P < 0.05$, $**P < 0.01$; ANOVA with post-hoc Bonferroni test. (d) We established 3 cohorts of 6 wild-type adult C57BL/6J mice, and performed daily intraperitoneal injections of KD3010 at 10 mg/kg or 50 mg/kg body weight (or injected vehicle only = 0 mg/kg) for 5 days. On day 6, mice were euthanized, and we measured PPARδ target gene expression in the striatum by qRT-PCR analysis. Results for each target gene are normalized to mice receiving diluent only. $*P < 0.05$; ANOVA with post-hoc Tukey test. (e) We weighed HD mice receiving vehicle or KD3010 from 6 weeks of age (Baseline) until 18 weeks of age. (f) We measured combined fore-limb / hind-limb grip strength for HD mice receiving vehicle or KD3010 from 6 weeks of age (Baseline) until 18 weeks of age. $***P < .001$, t-test. (g) Results for neurological screening tests that comprise the composite exam for HD mice on vehicle or KD3010 from 6 weeks of age (Baseline) until 18 weeks of age. Group sizes were: 9 Wild-type mice, 13 HD mice on vehicle, and 12 HD on KD3010. $*P < .05$, $***P < .001$, t-test. All experiments were performed in triplicate or quadruplicate. Error bars = s.e.m.

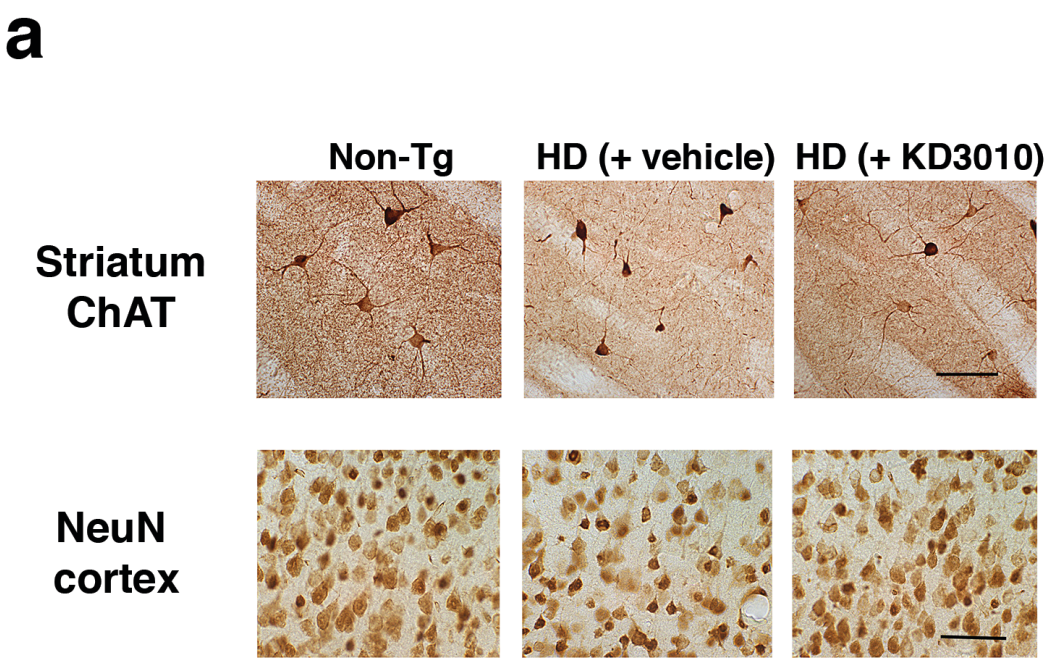


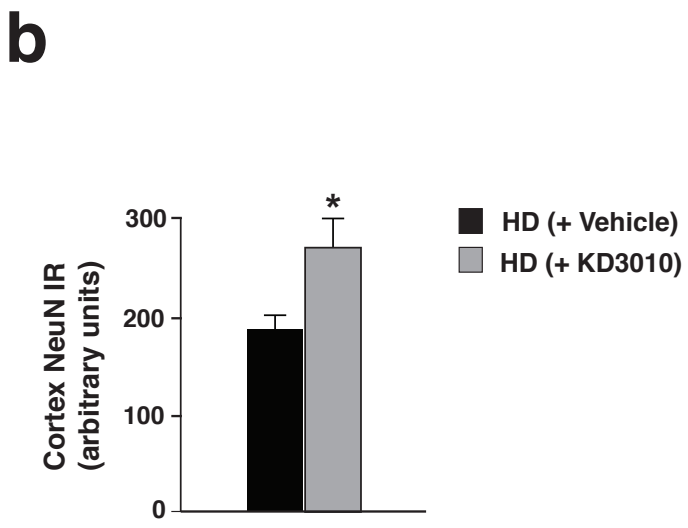


**Supplementary Figure 13**

**KD3010 prevents neurodegeneration in HD mice.**

(a) We immunostained sections of striatum for choline acetyltransferase (ChAT) and sections of cortex for NeuN from 18 week-old HD mice receiving vehicle or KD3010 (n = 4 mice / group). Retention of increased striatal ChAT immunoreactivity and of increased cortical NeuN immunoreactivity occurs in KD3010-treated HD mice. Scale bar = 50 μM.
(b) Quantification of cortical NeuN immunoreactivity (IR) shown in (a).
*$P < .05$, t-test. Error bars = s.e.m.